HHS Public Access

Author manuscript

Int J Obes (Lond). Author manuscript; available in PMC 2019 April 03.

Published in final edited form as:

Int J Obes (Lond). 2019 April ; 43(4): 906–916. doi:10.1038/s41366-018-0145-7.

Maternal high fat diet reversal improves placental hemodynamics in a nonhuman primate model of diet-induced obesity

Jennifer A. Salati, MD[1], **Victoria H.J. Roberts, PhD**[2], **Matthias C. Schabel, PhD**[3,4], **Jamie O. Lo, MD**[1], **Christopher D. Kroenke, PhD**[3,5], **Katherine S. Lewandowski, BS**[2], **Jonathan R. Lindner, MD**[6,7], **Kevin L. Grove, PhD**[8], and **Antonio E. Frias, MD**[1,2]

[1]Department of Obstetrics & Gynecology, Oregon Health & Science University, 3181 S.W. Sam Jackson Park Rd, Portland, OR 97239

[2]Division of Reproductive and Developmental Sciences, Oregon National Primate Research Center, Oregon Health & Science University, 505 NW 185th Ave, Beaverton, OR 97006

[3]Advanced Imaging Research Center, Oregon Health & Science University, 3181 S.W. Sam Jackson Park Rd, Portland, OR 97239

[4]Utah Center for Advanced Imaging Research, University of Utah, Salt Lake City, UT 84112

[5]Division of Neuroscience, Oregon National Primate Research Center, Oregon Health & Science University, Beaverton, 505 NW 185th Ave, Beaverton, OR 97006

[6]Knight Cardiovascular Institute, Oregon Health & Science University, 3303 S.W. Bond Ave., Portland, OR 97239

[7]Division of Cardiometabolic Health, Oregon National Primate Research Center, Oregon Health & Science University, 505 NW 185th Ave, Beaverton, OR 97006

[8]Novo Nordisk Research Center, 530 Fairview Ave N #5000, Seattle, WA 98109

Abstract

Background—In a Japanese macaque model of diet-induced obesity, we have previously demonstrated that consumption of a high fat, 'Western-style' diet (WSD) is associated with placental dysfunction and adverse pregnancy outcomes, independent of an obese maternal phenotype. Specifically, we have reported decreased uterine placental blood flow and increased inflammation with maternal WSD consumption. We also previously investigated the use of a promising therapeutic intervention that mitigated the adverse placental effects of a WSD but had unexpected detrimental effects on fetal pancreatic development. Thus, the objective of the current

Corresponding author: Victoria HJ Roberts; Division of Reproductive and Developmental Sciences, Oregon National Primate Research Center, Oregon Health & Science University, 505 NW 185th Ave, Beaverton, OR 97006. robertsv@ohsu.edu Phone number: 503-346-5431. Fax number: 503-346-5585.

Conflict of Interest: The authors report no conflicts of interest.

study was to determine whether simple preconception diet reversal would improve placental function.

Methods—Female Japanese macaques were divided in to three groups: diet reversal animals (n=5) were switched from a chronic WSD (36% fat) to a low fat, control diet (14% fat) prior to conception and throughout pregnancy. The control (n=6) and WSD (n=6) cohorts were maintained on their respective diets throughout pregnancy. Maternal body weight and composition were regularly assessed and advanced non-invasive imaging was performed at mid-gestation (gestational day 90, G90 or 0.5 of gestation, where full term is G175), and G129, one day prior to C-section delivery at G130 (0.75 of gestation). Imaging studies comprised Doppler ultrasound (US), Contrast-Enhanced US (CEUS) and Dynamic-Contrast-Enhanced Magnetic Resonance Imaging (DCE-MRI) to assess uteroplacental hemodynamics and maternal-side placental perfusion.

Results—Dietary intervention resulted in significant maternal weight loss prior to pregnancy, and improved lean to fat mass ratio. By advanced imaging we demonstrated that a chronic WSD led to decreased blood flow velocity in the intervillous space, delayed blood flow transfer through the maternal spiral arteries and reduced total placental blood flow compared to control fed animals. Dietary reversal ameliorated these concerning derangements, restoring these hemodynamic parameters to control levels.

Conclusion—Preconception dietary modification has beneficial effects on the maternal metabolic phenotype, and results in improved placental hemodynamics.

Introduction

Obesity is a major health issue in the United States, with over 35% of the population meeting criteria for obesity with a body mass index >30 kg/m^2.[1] This epidemic has contributed significantly to the rising healthcare burden of coronary artery disease, diabetes and hypertension. Paralleling this national trend, obesity complicates up to 20% of pregnancies in the United States,[2] and is associated with multiple adverse pregnancy outcomes, including gestational hypertension, preeclampsia, gestational diabetes, and stillbirth.[2,3] The mechanisms underlying these increased risks are incompletely understood, but placental dysfunction has been implicated in many of these complications.[4–6] The placenta is the primary organ for nutrient exchange during pregnancy, and abnormal placental development has been associated with most adverse obstetric outcomes including abnormalities in fetal growth, preterm labor, preeclampsia, and stillbirth.[5,7,8] In addition, obese gravidae demonstrate impaired vascular function when compared with lean counterparts, which may contribute to their increased risk of preeclampsia and placental dysfunction.[9] Although the cause of obesity is multifactorial, poor diet is a major contributor, with the majority of Americans consuming a “Western-style diet” (WSD) high in calories and saturated fats.

We have previously demonstrated in our nonhuman primate (NHP) model of chronic excess nutrition that consumption of a WSD during pregnancy reduces uterine blood flow and increases the risk of stillbirth.[10,11] The deleterious effects of a WSD were independent of obesity, though the degree of placental dysfunction was greater in the animals that were

obese and consuming a WSD. These results in the NHP support other studies in various animal models implicating obesity and overnutrition in placental dysfunction and poor obstetric outcomes.[12–14] In addition to the placenta, *in utero* WSD exposure also alters the normal development of key metabolic fetal organs in the early third trimester independent of maternal obesity, including the liver, brain, pancreas, and skeletal muscle.[15–18] In an effort to mitigate the deleterious effects of a WSD, our group previously investigated supplementation of the WSD with the polyphenol resveratrol as a potential therapeutic. Despite maternal and placental beneficial effects, we found an unexpected and concerning effect of resveratrol on fetal pancreatic development.[11] Thus alternative strategies are needed.

Unfortunately, the lack of noninvasive imaging modalities that facilitate the *in vivo* study of both normal and abnormal placental vascular perfusion impedes our understanding of placental vascular function and development, making the placenta the least understood human organ.[19] We have recently implemented advanced imaging methods to overcome the known limitations of standard Doppler ultrasound (D-US) to assess maternal-side placental blood flow. The first, contrast-enhanced ultrasound (CE-US), is a noninvasive technique that facilitates imaging of microvascular perfusion with the use of acoustic detection of gas-filled, lipid-encapsulated microbubble contrast agents.[20–22] The use of a contrast agent permits assessment of perfusion in small capillary networks that are difficult to assess solely with D-US. Utilizing this technology, we are able to calculate the microvascular flux rate constant, which is a measure of in-flow velocity, at the level of each individual maternal spiral artery. Although this is not an absolute measure of flow (volume/time), it is an estimate of impedance at the spiral artery. To measure total blood flow to the placenta, we have developed a Dynamic Contrast Enhanced Magnetic Resonance Imaging (DCE-MRI) method using a contrast agent that quantitatively measures blood flow to the placenta from all the spiral arteries filling the intervillous space.[23]

In this study, we investigated the impact of pre-pregnancy dietary reversal in NHPs on placental hemodynamics and blood flow kinetics using advanced imaging techniques. Since a WSD reduces uterine placental blood flow,[10] we hypothesized that switching NHPs from a chronic WSD to a standard chow diet prior to conception would alter intervillous blood flow hemodynamics and improve placental function.

Material and Methods

Non-human primate model

Female Japanese macaques (*macaca fuscata*, aged 6 – 15 years) were maintained on a WSD with 36% of calories from fat (Purina Mills, Inc., St. Louis, MO, USA) for at least 4 years (n=6). Control animals were maintained on a standard chow diet (CON, n=6) with 14% of calories from fat. The diet reversal cohort (REV, n=5) were maintained on a WSD for 4-7 years and then switched to a CON diet 3 months prior to the breeding season (Fig. 1A). All diets contained appropriate vitamin, mineral and protein content to support normal growth. Based on our prior published macaque studies,[11,24,25] a sample size of 5 or 6 animals per diet cohort was anticipated to provide adequate power for statistical analysis.

Animals were socially housed in groups of 8-10 females and 2 males per diet-determined cohorts in indoor/outdoor facilities with *ad libitum* access to food and water; thus animal selection was not randomized prior to the study. Animals bred naturally, and pregnancies were identified by monthly physicals during the breeding season. Gestational age was confirmed by ultrasonographic fetal biometry measurements in the early first trimester. All animal procedures were conducted in accordance with the guidelines of the Institutional Animal Care and Use Committee (IACUC) of the Oregon National Primate Research Center (ONPRC). The ONPRC abides by the Animal Welfare Act and Regulations enforced by the United States Department of Agriculture.

Maternal metabolic parameters

Maternal body weight was measured prior to pregnancy and at regular intervals throughout pregnancy. Body composition for each animal was determined by dual-energy X-ray absorptiometry (DEXA) scans (Hologic QDR Discovery A; Hologic, Inc., Bedford, MA, USA) prior to pregnancy and in the postpartum period. Total body scans were performed in supine position under Telazol sedation (3-5 mg/kg intramuscular; Fort Dodge Animal Health, Pfizer, NY, USA), and QDR software used to calculate body composition. Maternal whole blood was collected from the femoral artery at gestational day (G)120 (0.7 of gestation) after overnight food withdrawal, and plasma and serum were isolated by centrifugation. Serum cholesterol, low-density lipoprotein (LDL), and triglyceride measurements were assayed by the Endocrine Technology and Support Core Laboratory at the ONPRC using a Horiba ABX Pentra 400 Clinical Chemistry System (Horiba Medical, Irvine, CA, USA).

Imaging studies

Placental imaging was performed at G90 (0.5 of gestation) and G129 (0.75 of gestation, the early third trimester). Animals were initially sedated with 3-5 mg/kg of intramuscular Telazol, intubated and maintained under anesthesia with 1-2% isoflurane gas for the duration of the examination. Intravenous Flumazenil (APP Pharmaceuticals, Schaumburg, IL, USA) at 0.01 mg/kg was given following isoflurane administration to facilitate hemodynamic stabilization.[26] Animals were placed in dorsal recumbent position and underwent physiologic vital sign monitoring for the duration of the procedure. All animals experienced the same sedation protocol and remained hemodynamically stable throughout the imaging procedures. For each imaging study, the ultrasonographer (AEF) and MRI operator (MCS) were blinded to animal experimental group.

Doppler ultrasound

Image-directed pulsed and color Doppler equipment (GE Voluson 730 Expert, Kretztechnik, Zipf, Austria) with a 5- to 9-MHz sector probe was used. The lowest high-pass filter level (100 Hz), and an angle of 15° or less between the vessel and Doppler beam was considered acceptable. Uterine artery blood flow velocity waveforms were obtained from the proximal portion of the uterine artery as described previously.[10,11,27,28] The cross-sectional area (CSA) of the vessel was calculated as $CSA = \pi(d/2)^2$, where d=diameter. The calculated uterine artery volume blood flow (cQ_{uta}), which estimates blood flow through the uterine artery, was calculated as the velocity-time integral × CSA × fetal heart rate and normalized

by maternal weight in kilograms. Pulsatility index (PI) was calculated from waveforms obtained from the uterine artery and the umbilical artery in a free loop of umbilical cord.

Contrast-enhanced ultrasound

Contrast-enhanced ultrasound was performed with a Sequoia System (Siemens Medical Systems, Mountain View, CA, USA) using a 15L8 transducer at 7MHz with a 0.18 resting mechanical index (MI), and a 55dB dynamic range as previously described.[21,22] In brief, microbubble contrast reagent composed of lipid-shelled octofluoropropane was prepared in 0.9% normal saline to a concentration of 5% (Definity, Lantheus Medical Imaging, Billerica, MA, USA), and administered by continuous intravenous infusion at 60 ml/hr in the left upper extremity. Individual spiral arteries supplying a placental cotyledon were identified and centered directly beneath the ultrasound probe. A 2-second acoustic pulse (MI 1.9) was applied to destroy the microbubbles in the acoustic beam path, and microbubble re-entry into the intervillous space (IVS) was recorded at 1 frame per 75 milliseconds (ms) for rapidly re-filling vessels, or 1 frame per 125 ms for slower re-filling vessels until the area of interest reached signal saturation. Three sequential replicate recordings were taken for each identified region of interest (ROI). Analysis was performed using a CEUS analysis program. Blood flow kinetics within the IVS were assessed with manually specified ROI encompassing individual cotyledons. A kinetic curve was generated by fitting the data to the function $y=A(1-e^{-\beta t})$, where y is the video intensity (VI) at the pulsing interval t (ms), A is the VI plateau and β is the flux rate constant (FRC, s^{-1}). The FRC represents the mean microbubble transfer rate within the IVS and therefore reflects the blood velocity.[20] The spiral artery transit time (SAT) was defined as the time from microbubble destruction to observed initial cotyledon filling, or the time required for blood to flow through the spiral artery to the IVS (ms).

Dynamic Contrast Enhanced Magnetic Resonance Imaging (DCE-MRI)

MRI studies were performed on a nonhuman primate-dedicated 3T Siemens TIM-Trio scanner (Erlangen, Germany) using a circularly-polarized (CP) transmit, 15-channel receive radiofrequency (RF) “extremity” coil (QED, Cleveland, OH) as previously detailed.[23] Following localization of the placenta and acquisition of T2-weighted half-Fourier acquisition single-shot turbo spin-echo (HASTE) anatomic images in the coronal and axial planes, axial 2D multislice spoiled gradient echo (SPGR) images spanning the entire uterus, were acquired at six in-phase echo times with monopolar readout gradients. Subsequently, 3D SPGR images were acquired in the coronal plane to allow estimation of T1 (longitudinal relaxation time) with the variable flip angle (VFA) method.[29] Immediately after acquisition of VFA data, 150 volumes of 3D SPGR images were acquired for DCE-MRI with field of view and resolution matched to the VFA images. Ten baseline images were acquired prior to intravenous injection of a standard dose of 0.1 mmol/kg of gadoteridol CR (Prohance, Bracco Diagnostics Inc, Princeton, NJ) at a rate of 30 mL/min using a syringe pump (Harvard Apparatus, Holliston, MA).[30,31] Anatomic and multiecho imaging was performed during expiratory breath holding, achieved by temporarily suspending ventilation, while DCE-MRI data were acquired during ventilated free breathing. Physiological monitoring of pulse rate, arterial blood oxygen saturation, and respiration rate and end-tidal CO_2 partial pressure was performed throughout each MRI study.

Placental tissue collection

Cesarean section was performed at G130 (0.75 of gestation) in the ONPRC Surgical Services Unit. This time point is equivalent to the early third trimester and was chosen to facilitate optimal sample collection for multiple concurrent fetal experiments. The fetal weight and total weight of the two placental lobes was recorded. Individual placental cotyledons were weighed and their volume measured by saline displacement. Two full thickness (fetal membranes to maternal decidua) biopsy samples were obtained from each placental cotyledon, fixed in formalin and paraffin-embedded for stereological analysis. Villous tissue was collected from each individual placental cotyledon and flash frozen in liquid N_2 for later analysis.

Placental stereology

Each fixed placental tissue sample was serially sectioned into two series of eight sections (5μm thickness) with 100μm of tissue discarded between the two series. Two sections per tissue sample (4 sections per cotyledon) were stained using standard hematoxylin and eosin (H&E) methods. Digital images of stained sections were obtained with a virtual microscopy slide scanner (Olympus, Center Valley, PA, USA). Placental tissue structure was assessed by stereological analysis using newCAST™ software (Visiopharm, Hoersholm, Denmark). Systematic uniform random sampling was employed to identify tissue areas for analysis within each slide, and a grid of randomly superimposed geometric point probes were utilized to count placental structures. Blinded stereology analysis was performed at 10× magnification, and volume fractions of the villi and IVS were determined.[32] Tissue shrinkage factor in fixed and processed tissues can be calculated using red blood cells as a size marker. This was not calculated in the current study, however all tissue sections were processed with standardized methods and fixation duration to reduce variability in data end points due to shrinkage.

Placental inflammation

Frozen placental villous tissue samples were homogenized in lysis buffer (20mM Tris with pH 7.5, 1mM EDTA, 1mM EGTA, 20mM sodium fluoride, 0.15M sodium chloride, 0.5% Nonidet P-40, 0.5% Triton X-100, 200μM sodium orthovanadate, 2μM leupeptin, 5.8μM pepstatin, 200μM 4-(2-aminoethyl) benzenesulfonyl fluoride hydrochloride, and 5μM N-tosyl-L-lysine chloromethyl ketone) and centrifuged for 5 minutes at 20,000 × g to remove cell debris. Inflammatory markers were assessed with a commercially available antibody array (Abcam, Cambridge, MA, USA) using pooled placental samples from each dietary group. Enzyme-linked immunosorbent assay (ELISA) kits [TNFα, Life Technologies, Carlsbad, CA, USA; IL-12, Invitrogen Life Technologies, Grand Island, NY, USA; [regulated on activation, normal T-cell expressed and secreted (RANTES)], Thermo Scientific, Rockford, IL, USA; IL-1ß, Invitrogen Life Technologies, Grand Island, NY, USA] were used to assess selected inflammatory markers. Assays were performed according to the manufacturers' instructions and expression levels derived from known standards. Reported data was corrected for protein content determined by BCA assay (Thermo Scientific, Rockford, IL, USA).

Statistical analysis

Data are expressed as mean ± standard error of the mean (SEM), and analysis performed using statistical analysis software (GraphPad Prism, La Jolla, CA). Differences in mean body weight at multiple time points within the REV group were compared using a Friedman test followed by Dunn's multiple comparisons test. Differences between the three diet groups (CON, WSD, REV) were analyzed using a Kruskal-Wallis test followed by Dunn's multiple comparisons test. Within each diet group, differences between G90 and G129 were compared using the Mann-Whitney test. A P-value <0.05 was considered statistically significant.

Results

Diet reversal improves the maternal phenotype

In the pre-conception period, the REV dams were significantly heavier than the CON dams (Fig. 1B, $p<0.001$). Following dietary intervention, the REV dams experienced a 20% weight loss (Fig. 1C), and were comparable in weight to the WSD dams at the time of conception (Fig. 1B). Appropriate weight gain was observed throughout pregnancy in all diet groups. By the third trimester, the REV dams remained comparable in weight to the WSD dams, although were significantly heavier than CON animals ($p<0.01$). Prior to pregnancy, the mean ratio of fat to lean mass was higher in REV dams compared to CON dams (Fig. 1D, $p<0.01$). Following pregnancy, the fat to lean mass in the REV cohort had decreased and was comparable to both WSD and CON animals.

Maternal serum cholesterol and LDL levels at 0.7 of gestation were comparable between diet groups (Fig. 1E-F). Maternal serum triglyceride levels were increased two-fold with WSD compared to CON (Fig. 1G) and reduced to control levels in the diet reversal cohort.

Diet reversal mitigates perturbed placental perfusion observed with WSD consumption

Total blood flow to both placental lobes was quantified by DCE-MRI at G90 and G129 (0.5 and 0.75 of gestation respectively). We observed a modest increase in total blood flow from mid-gestation to the early third trimester in all groups (Fig. 2A) but significantly diminished flow in the WSD animals at both time points compared to CON ($p<0.05$). Placental blood flow was restored to CON levels in the REV cohort (Fig. 2).

Additionally, uteroplacental hemodynamics were investigated using Doppler ultrasound at G90 and G129. The uterine artery PI, an estimate of vascular impedance, was stable throughout gestation in all diet groups, and was comparable between groups with no differences between CON, WSD and REV groups at either G90 or G129 (Fig. 3A). The mean umbilical artery PI did not change significantly from G90 to G129 in either the CON or REV cohort (Fig. 3B). However, we did detect a 42% decrease in PI from G90 to G129 in our WSD cohort. The umbilical artery PI did not differ between diet groups at either gestational time point. The calculated uterine artery volume blood flow (cQ_{Uta}), normalized to maternal weight, did not change significantly from G90 to G129 in any of our cohorts (Fig. 3C). We were also unable to detect any significant differences in cQ_{Uta} between our dietary groups at either G90 or G129 (Fig. 3A).

Interrogation of spiral artery perfusion was achieved using Contrast-enhanced ultrasound. Analysis of kinetic curves allowed for the direct determination of the flux rate constant (FRC) and spiral artery transit time (SAT). Multiple cotyledons were analyzed in each animal study, and data reported as pooled values for each diet group at the two gestational time points. The total number of cotyledons analyzed per diet group at each time point were: CON G90 (n=28), CON G129 (n=26), WSD G90 (n=19), WSD G129 (n=28), REV G90 (n=23), REV G129 (n=25).

The FRC increased by 92% from G90 to G129 in CON dams (Fig. 4A, $p<0.05$). This effect was blunted in the WSD group, with a FRC at G90 that was comparable to CON dams, but no observed increase across gestation. Diet reversal resulted in a 69% increase in FRC compared to WSD at G90 ($p<0.05$), and a 2-fold increase in FRC at G129 ($p<0.005$).

The SAT was stable across gestation from G90 to G129 in all diet cohorts (Fig.4B). However, WSD resulted in prolongation of the SAT at G129 compared to CON dams. Diet reversal restored the SAT to CON levels at G129, with a 58% reduction in SAT compared to WSD dams.

Gross fetal and placental structural measures were not affected by WSD or diet reversal

The weights of fetal offspring taken at the time of necropsy (G130) did not differ between groups (Table 1). There was no difference in overall placental weight or volume between groups, and the mean number of placental cotyledons and mean cotyledon volume were similar. The feto:placental mass ratio, a measure of placental efficiency, did not differ between diet groups. Overall, mean villous and IVS volume were similar between diet groups (Table 1). Additionally, there were no differences in the absolute volume of fetal capillary or trophoblast in a subset of analyzed samples (n=3 animals/diet cohort, Table 1).

Placental inflammation

A WSD resulted in overall upregulation of multiple placental inflammatory markers, including TNFα, IL-12, IL-1β and RANTES (Fig. 5). Diet reversal reduced placental inflammation to mean levels comparable to controls. Selected confirmatory comparisons by ELISA revealed similar trends that did not reach statistical significance (Fig. 5).

Discussion

Utilizing advanced imaging to overcome known limitations in assessment of placental function *in vivo*, in this study we demonstrate perturbations of placental blood flow hemodynamics that are mitigated by dietary reversal in our WSD model. Specifically, by DCE-MRI we demonstrated decreased total maternal-side placental blood flow. The advantage of DCE-MRI is that it measures tissue perfusion of the placenta directly by measuring blood from each individual spiral artery through the entire volume of the placenta. Importantly, this method overcomes utilizing calculated uterine artery volumetric blood flow (in a large maternal vessel proximal to the placenta) as a proxy for placental microvascular tissue perfusion. DCE-MRI confirms, in this smaller cohort, the prior observations of disrupted placental hemodynamics on the maternal side of the placenta with WSD.[10,11]

The CEUS measures of spiral artery hemodynamics provide additional insight by providing a method to interrogate transit time through the spiral arteries and in-flow velocity of blood flow to the placenta. Spiral artery transit time was increased with WSD which could be secondary to the decreased total blood flow measured by DCE-MRI. Similarly, decreased in-flow velocity was also apparent in the WSD cohort and improved with REV. While the mechanisms for disruption of these parameters at the level of spiral artery in-flow to the placenta are not known several possibilities exist and merit further investigation. First, these measures could be affected by the decrease in total perfusion in the placenta measured by DCE-MRI. Second, we could speculate that a chronic WSD and dietary reversal may result in structural differences at the level of the spiral artery (vessel caliber or tortuosity) and the IVS, which could affect the velocity of blood transfer detected by CEUS. One technical limitation of CEUS when used to interrogate the placenta is the inability to assess fetal-side placental blood flow which is an important consideration for nutrient uptake and gaseous exchange at the materno-fetal interface. The close apposition of the two circulations makes the fetal vasculature susceptible to altered maternal flow parameters[33,34], however our stereological analysis did not reveal differences in the villous volume or the proportion of fetal capillary and trophoblast within the placental tissue. This does not exclude the possibility that remodeling of maternal spiral arteries is adversely impacted by WSD exposure, and that changes in the placental villous architecture may be too subtle to detect using 2 dimensional stereological assessment. Third, chronic inflammation within the spiral artery, at the level of the trophoblast, or endothelial cell activation of the spiral arteries could affect blood flow as has been reported in other blood vessels in this model.[35] We demonstrate some evidence of increased inflammation in the current study, and have previously demonstrated increased expression of placental pro-inflammatory mediators with a WSD in the NHP.[10,11]

The Japanese macaque model of diet-induced obesity has been used for more than a decade and our collaborative group have investigated multiple aspects of maternal WSD consumption in relation to fetal and juvenile outcomes. We have demonstrated fetal liver lipotoxicity[15] and hepatic inflammation,[36] decreased oxidative metabolism in fetal muscle,[16] impaired islet vascularization[18] and increased pancreatic inflammation,[17] in addition to our reports of perturbed placental function and development.[10,11] The current study demonstrated positive effects of a dietary intervention on maternal body weight, composition and circulating triglycerides. This observation is clinically pertinent, as human studies have shown that a lower pre-pregnancy weight is associated with decreased adverse pregnancy outcomes.[8,37] Additionally, although the complex relationships between maternal obesity, overnutrition, pregnancy outcomes and offspring health are not well understood, maternal obesity and WSD consumption are causal factors for long-term risk of obesity and metabolic dysfunction in offspring.[38,39] Importantly, we have reported that impairments in fetal pancreatic development are mitigated by diet reversal,[18] reducing offspring susceptibility to type II diabetes in later life. Similarly, placental hemodynamic function was improved with dietary reversal despite persistence of a maternal obesity compared to controls.

In conclusion, here we show that diet reversal improves placental function in our nonhuman primate model of diet-induced obesity utilizing advanced imaging. Preconception diet reversal is a feasible and inexpensive intervention that addresses a modifiable risk factor for

poor pregnancy outcomes, with suggested improvements in metabolic programming of the offspring.[18] Perhaps the greatest barrier to effective use is that only the minority of women present to an obstetric provider for preconception counseling, and the majority seek initial care in the middle of the first trimester, at which time rapid and significant weight loss is not recommended. Therefore, all women of reproductive age who present in any capacity to primary care should be counseled about the importance of maintaining a healthy diet and lifestyle, and the implications of poor diet and obesity on pregnancy outcomes. Furthermore, continued innovation in functional *in vivo* imaging will aid our understanding of placental development, and facilitate effective clinical interventions during at-risk pregnancies.

Acknowledgments

The authors thank Diana Takahashi, Karalee Baquero, Jessica Walker, Peter Blundell and Tyler Dean (Oregon National Primate Research Center) for technical assistance and guidance with the animal studies.

Funding sources: Supported by NIH #R21HD076265, and NIH #R24DK0909640. In addition, research reported in this publication was supported by the Office of the Director, National Institutes of Health of the National Institutes of Health under Award Number P51OD011092. The content is solely the responsibility of the authors and does not necessarily represent the official views of the National Institutes of Health.

References

1. Ogden, CL, Carroll, MD, Kit, BK, Flegal, KM. NCHS Data Brief. 2012. Prevalence of obesity in the United States, 2009-2010; 1–8.
2. Fisher SC, Kim SY, Sharma AJ, Rochat R, Morrow B. Is obesity still increasing among pregnant women? Prepregnancy obesity trends in 20 states, 2003-2009. Prev Med. 2013; 56(6):372–378. [PubMed: 23454595]
3. Schummers L, Hutcheon JA, Bodnar LM, Lieberman E, Himes KP. Risk of adverse pregnancy outcomes by prepregnancy body mass index: a population-based study to inform prepregnancy weight loss counseling. Obstet Gynecol. 2015; 125(1):133–143. [PubMed: 25560115]
4. Kidron D, Bernheim J, Aviram R. Placental findings contributing to fetal death, a study of 120 stillbirths between 23 and 40 weeks gestation. Placenta. 2009; 30(8):700–704. [PubMed: 19535137]
5. Nohr EA, Bech BH, Davies MJ, Frydenberg M, Henriksen TB, Olsen J. Prepregnancy obesity and fetal death: a study within the Danish National Birth Cohort. Obstet Gynecol. 2005; 106(2):250–259. [PubMed: 16055572]
6. Roberts DJ, Post MD. The placenta in pre-eclampsia and intrauterine growth restriction. J Clin Pathol. 2008; 61(12):1254–1260. [PubMed: 18641412]
7. Challier JC, Basu S, Bintein T, et al. Obesity in pregnancy stimulates macrophage accumulation and inflammation in the placenta. Placenta. 2008; 29(3):274–281. [PubMed: 18262644]
8. Cnattingius S, Bergstrom R, Lipworth L, Kramer MS. Prepregnancy weight and the risk of adverse pregnancy outcomes. N Engl J Med. 1998; 338(3):147–152. [PubMed: 9428815]
9. Stewart FM, Freeman DJ, Ramsay JE, Greer IA, Caslake M, Ferrell WR. Longitudinal assessment of maternal endothelial function and markers of inflammation and placental function throughout pregnancy in lean and obese mothers. J Clin Endocrinol Metab. 2007; 92(3):969–975. [PubMed: 17192290]
10. Frias AE, Morgan TK, Evans AE, et al. Maternal high-fat diet disturbs uteroplacental hemodynamics and increases the frequency of stillbirth in a nonhuman primate model of excess nutrition. Endocrinology. 2011; 152(6):2456–2464. [PubMed: 21447636]
11. Roberts VH, Pound LD, Thorn SR, et al. Beneficial and cautionary outcomes of resveratrol supplementation in pregnant nonhuman primates. FASEB J. 2014; 28(6):2466–2477. [PubMed: 24563374]

12. Hayes EK, Lechowicz A, Petrik JJ, et al. Adverse fetal and neonatal outcomes associated with a life-long high fat diet: role of altered development of the placental vasculature. PLoS One. 2012; 7(3):e33370. [PubMed: 22442686]
13. Liang C, DeCourcy K, Prater MR. High-saturated-fat diet induces gestational diabetes and placental vasculopathy in C57BL/6 mice. Metabolism. 2010; 59(7):943–950. [PubMed: 20022072]
14. Wallace JM, Bourke DA, Aitken RP, Palmer RM, Da Silva P, Cruickshank MA. Relationship between nutritionally-mediated placental growth restriction and fetal growth, body composition and endocrine status during late gestation in adolescent sheep. Placenta. 2000; 21(1):100–108. [PubMed: 10692257]
15. McCurdy CE, Bishop JM, Williams SM, et al. Maternal high-fat diet triggers lipotoxicity in the fetal livers of nonhuman primates. J Clin Invest. 2009; 119(2):323–335. [PubMed: 19147984]
16. McCurdy CE, Schenk S, Hetrick B, et al. Maternal obesity reduces oxidative capacity in fetal skeletal muscle of Japanese macaques. JCI Insight. 2016; 1(16):e86612. [PubMed: 27734025]
17. Nicol LE, Grant WF, Comstock SM, et al. Pancreatic inflammation and increased islet macrophages in insulin-resistant juvenile primates. J Endocrinol. 2013; 217(2):207–213. [PubMed: 23420316]
18. Pound LD, Comstock SM, Grove KL. Consumption of a Western-style diet during pregnancy impairs offspring islet vascularization in a Japanese macaque model. Am J Physiol Endocrinol Metab. 2014; 307(1):E115–123. [PubMed: 24844258]
19. Guttmacher AE, Maddox YT, Spong CY. The Human Placenta Project: placental structure, development, and function in real time. Placenta. 2014; 35(5):303–304. [PubMed: 24661567]
20. Kaufmann BA, Wei K, Lindner JR. Contrast echocardiography. Curr Probl Cardiol. 2007; 32(2): 51–96. [PubMed: 17208647]
21. Roberts VH, Lo JO, Salati JA, et al. Quantitative assessment of placental perfusion by contrast-enhanced ultrasound in macaques and human subjects. Am J Obstet Gynecol. 2016; 214(3):369 e361–368. [PubMed: 26928151]
22. Roberts VHJ, Lo JO, Lewandowski KS, et al. Adverse Placental Perfusion and Pregnancy Outcomes in a New Nonhuman Primate Model of Gestational Protein Restriction. Reprod Sci. 2017
23. Frias AE, Schabel MC, Roberts VH, et al. Using dynamic contrast-enhanced MRI to quantitatively characterize maternal vascular organization in the primate placenta. Magn Reson Med. 2015; 73(4):1570–1578. [PubMed: 24753177]
24. Lo JO, Schabel MC, Roberts VH, et al. Vitamin C supplementation ameliorates the adverse effects of nicotine on placental hemodynamics and histology in nonhuman primates. Am J Obstet Gynecol. 2015; 212(3):370 e371–378. [PubMed: 25725660]
25. Roberts VH, Rasanen JP, Novy MJ, et al. Restriction of placental vasculature in a non-human primate: a unique model to study placental plasticity. Placenta. 2012; 33(1):73–76. [PubMed: 22030304]
26. Lee JY, Kim MC. Anesthesia of growing pigs with tiletamine-zolazepam and reversal with flumazenil. J Vet Med Sci. 2012; 74(3):335–339. [PubMed: 22067078]
27. Acharya G, Sitras V, Erkinaro T, et al. Experimental validation of uterine artery volume blood flow measurement by Doppler ultrasonography in pregnant sheep. Ultrasound Obstet Gynecol. 2007; 29(4):401–406. [PubMed: 17390334]
28. Konje JC, Kaufmann P, Bell SC, Taylor DJ. A longitudinal study of quantitative uterine blood flow with the use of color power angiography in appropriate for gestational age pregnancies. Am J Obstet Gynecol. 2001; 185(3):608–613. [PubMed: 11568786]
29. Schabel MC, Morrell GR. Uncertainty in T(1) mapping using the variable flip angle method with two flip angles. Phys Med Biol. 2009; 54(1):N1–8. [PubMed: 19060359]
30. Oh KY, Roberts VH, Schabel MC, Grove KL, Woods M, Frias AE. Gadolinium Chelate Contrast Material in Pregnancy: Fetal Biodistribution in the Nonhuman Primate. Radiology. 2015; 276(1): 110–118. [PubMed: 25763829]
31. Prola-Netto J, Woods M, Roberts VHJ, et al. Gadolinium Chelate Safety in Pregnancy: Barely Detectable Gadolinium Levels in the Juvenile Nonhuman Primate after in Utero Exposure. Radiology. 2017:162534.

32. Mayhew TM, Burton GJ. Methodological problems in placental morphometry: apologia for the use of stereology based on sound sampling practice. Placenta. 1988; 9(6):565–581. [PubMed: 3070535]

33. Chernyavsky IL, Leach L, Dryden IL, Jensen OE. Transport in the placenta: homogenizing haemodynamics in a disordered medium. Philos Trans A Math Phys Eng Sci. 2011; 369(1954): 4162–4182. [PubMed: 21969671]

34. Mayhew TM, Charnock-Jones DS, Kaufmann P. Aspects of human fetoplacental vasculogenesis and angiogenesis. III. Changes in complicated pregnancies. Placenta. 2004; 25(2–3):127–139. [PubMed: 14972445]

35. Chadderdon SM, Belcik JT, Bader L, et al. Proinflammatory endothelial activation detected by molecular imaging in obese nonhuman primates coincides with onset of insulin resistance and progressively increases with duration of insulin resistance. Circulation. 2014; 129(4):471–478. [PubMed: 24163066]

36. Grant WF, Nicol LE, Thorn SR, Grove KL, Friedman JE, Marks DL. Perinatal exposure to a high-fat diet is associated with reduced hepatic sympathetic innervation in one-year old male Japanese macaques. PLoS One. 2012; 7(10):e48119. [PubMed: 23118937]

37. Rosenberg TJ, Garbers S, Chavkin W, Chiasson MA. Prepregnancy weight and adverse perinatal outcomes in an ethnically diverse population. Obstet Gynecol. 2003; 102(5 Pt 1):1022–1027. [PubMed: 14672480]

38. Armitage JA, Taylor PD, Poston L. Experimental models of developmental programming: consequences of exposure to an energy rich diet during development. J Physiol. 2005; 565(Pt 1):3–8. [PubMed: 15695245]

39. Whitaker RC, Wright JA, Pepe MS, Seidel KD, Dietz WH. Predicting obesity in young adulthood from childhood and parental obesity. N Engl J Med. 1997; 337(13):869–873. [PubMed: 9302300]

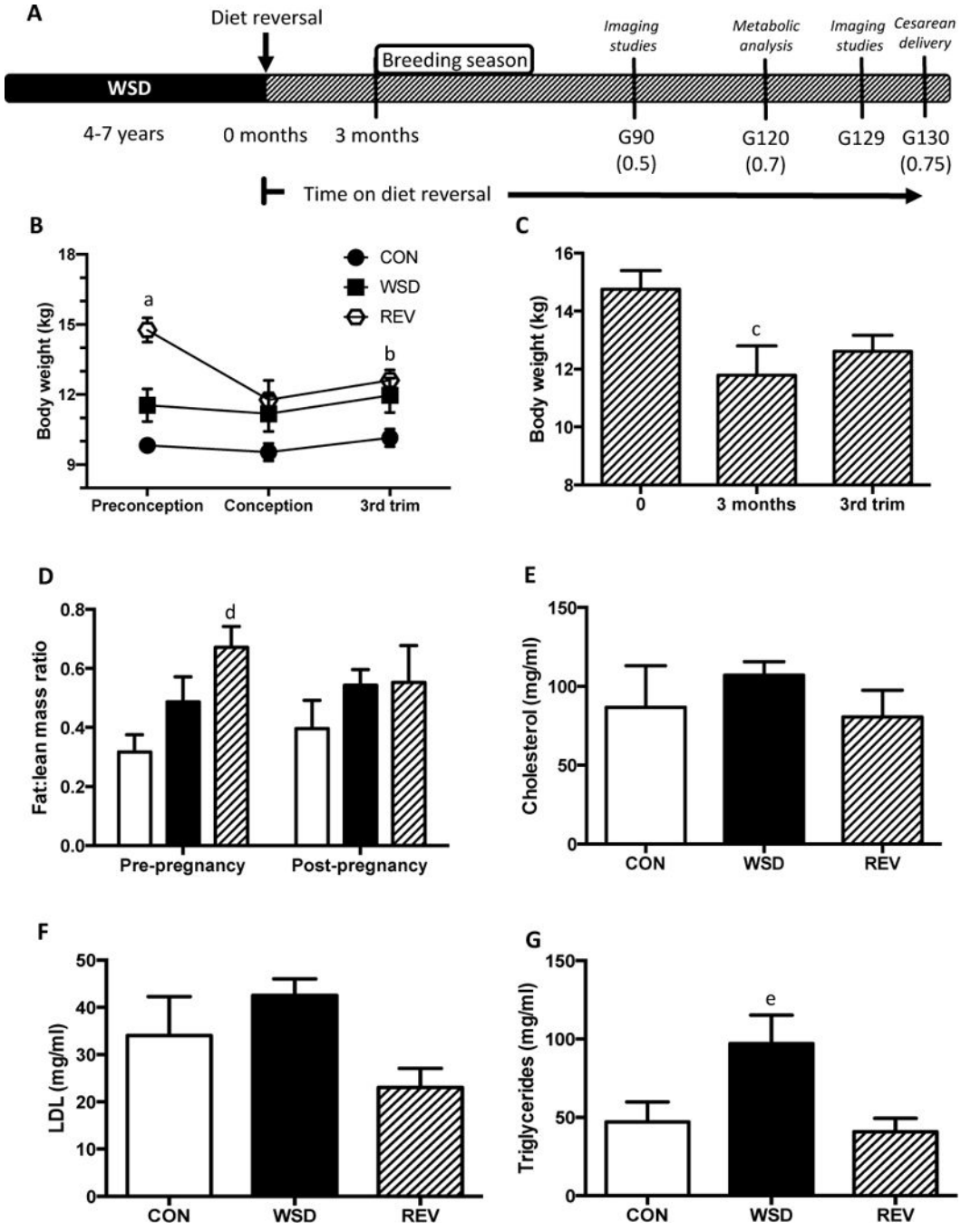

Figure 1. Study design and maternal metabolic parameters

A. Schematic representation of the study design indicating data collection time points with the proportion of gestation (0.5, 0.7 and 0.75) given in parentheses.

B. Body weight in all groups at preconception through the third trimester. C. Body weight in the diet reversal group at preconception (0=initiation of diet intervention), 3 months after dietary intervention, and third trimester (G130). D. Fat-to-lean mass ratio determined by dual-energy X-ray absorptiometry scan pre- and post-pregnancy. E. Cholesterol levels, F. Low density lipoprotein levels, and G. Triglyceride levels at G120. Data are presented as the

mean ± standard error of the mean for each diet group (CON, n=6; WSD, n=6; REV, n=5). [a]p<0.001 REV *vs.* CON; [b]p<0.01 REV *vs.* CON, Kruskal-Wallis test; [c]p<0.013 months *vs.*0 months, Friedman test; [d]p<0.05 REV *vs.* CON; [e]p=0.007 WSD *vs.* CON, Kruskal-Wallis test.

G, gestational day; CON, control; WSD, Western-style diet; REV, diet reversal; trim, trimester; LDL, low density lipoprotein.

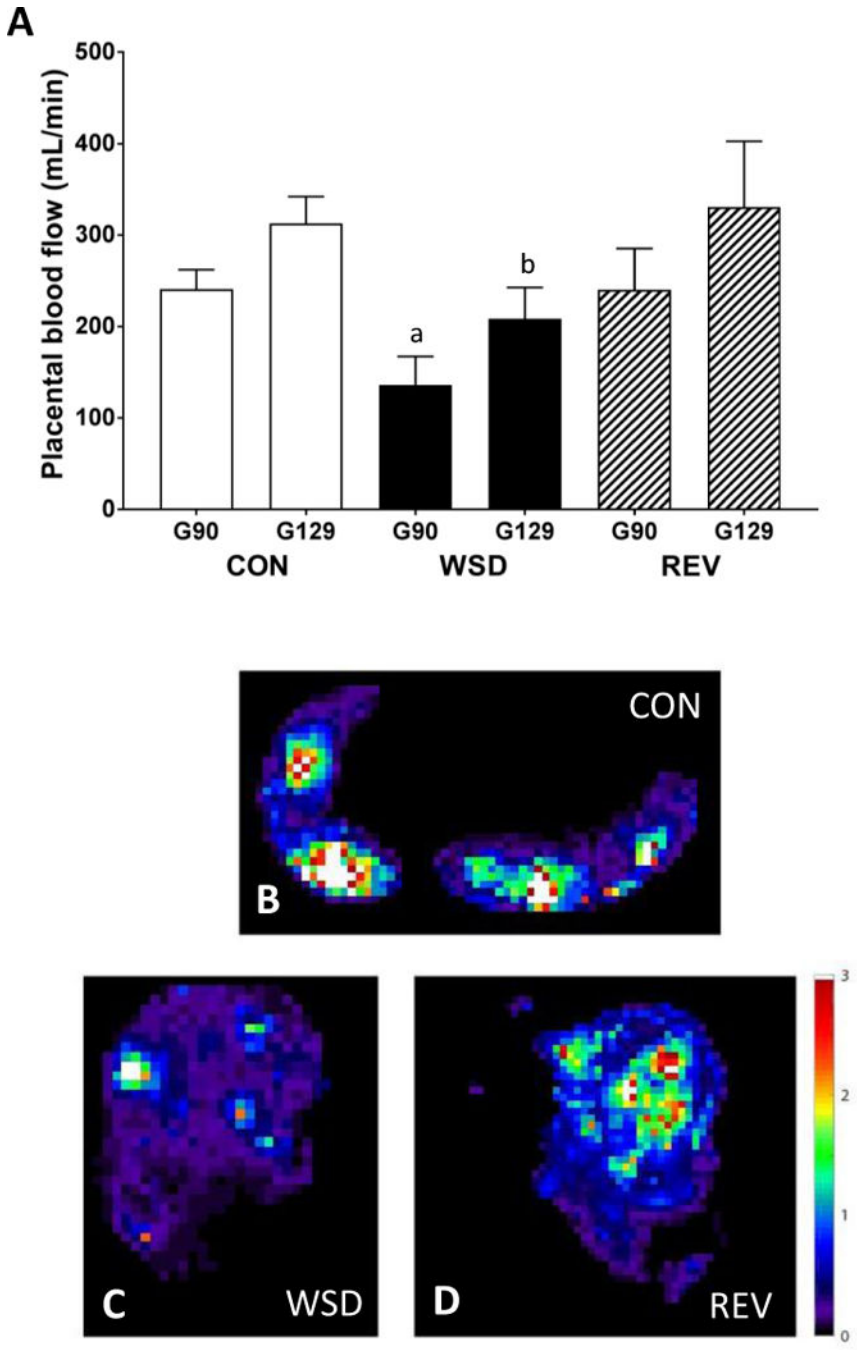

Figure 2. Dynamic Contrast-Enhanced MRI

A. Total placental blood flow quantified by DCE-MRI at gestational days 90 and 129 in CON (n=6), WSD (n=6) and REV (n=5) animals. Data are presented as mean ± standard error of the mean. [a]p<0.05 *vs.* G90 CON; [b]p<0.05 *vs.* G129 CON. Placental blood flow (measured in ml blood/ml placenta/minute) as quantified by DCE-MRI for an imaging section through the placenta in a single representative animal from each of our three groups: CON (B), WSD (C), and REV (D).

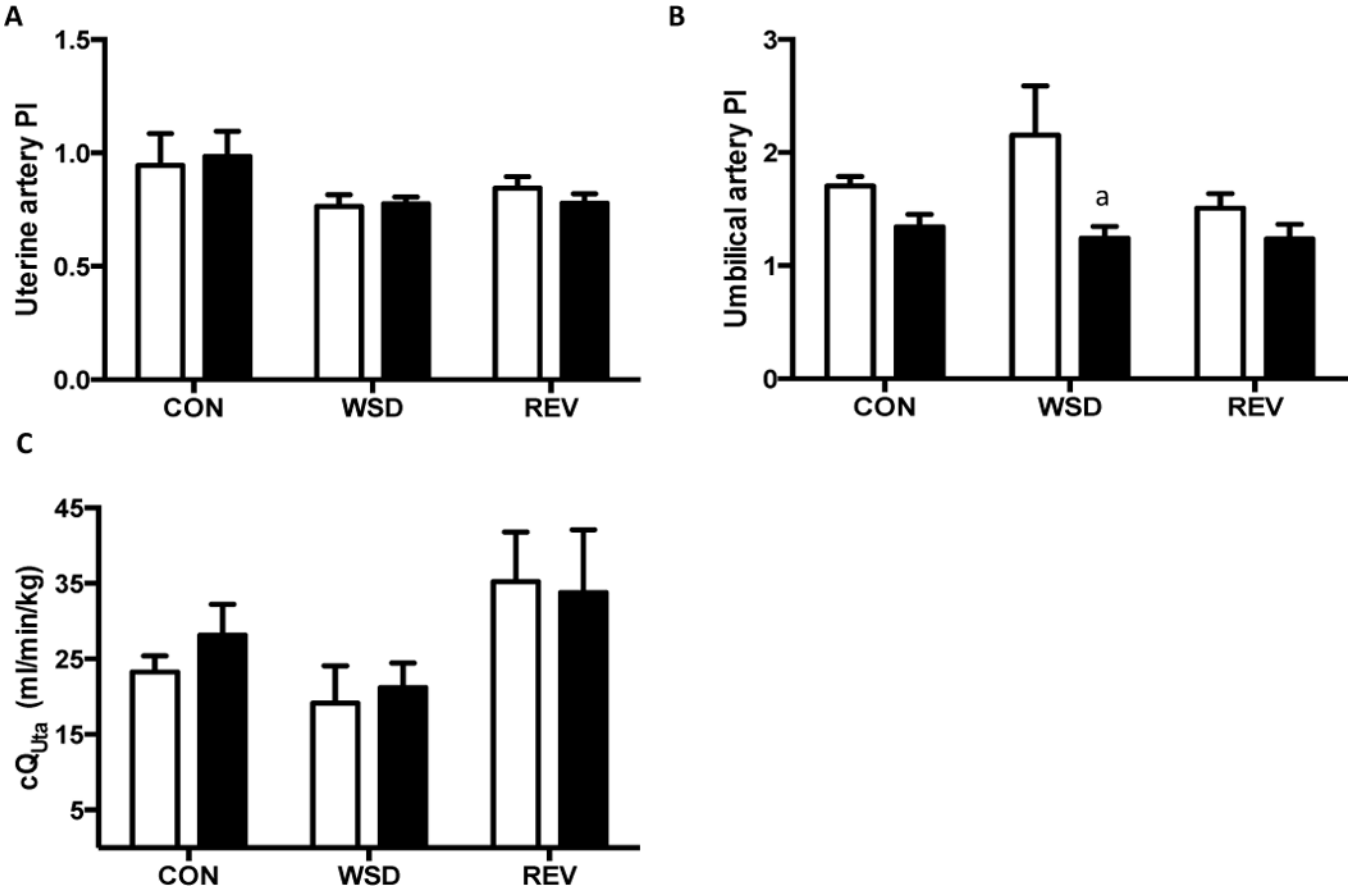

Figure 3. Doppler ultrasound

A. Uterine artery PI. B. Umbilical artery PI. C. Calculated uterine artery volume blood flow (cQ_{uta}) corrected for maternal body weight. $^{a}p<0.05$ G129 *vs.* G90, Mann-Whitney test. Open bars, G90; closed bars, G129; PI, pulsatility index.

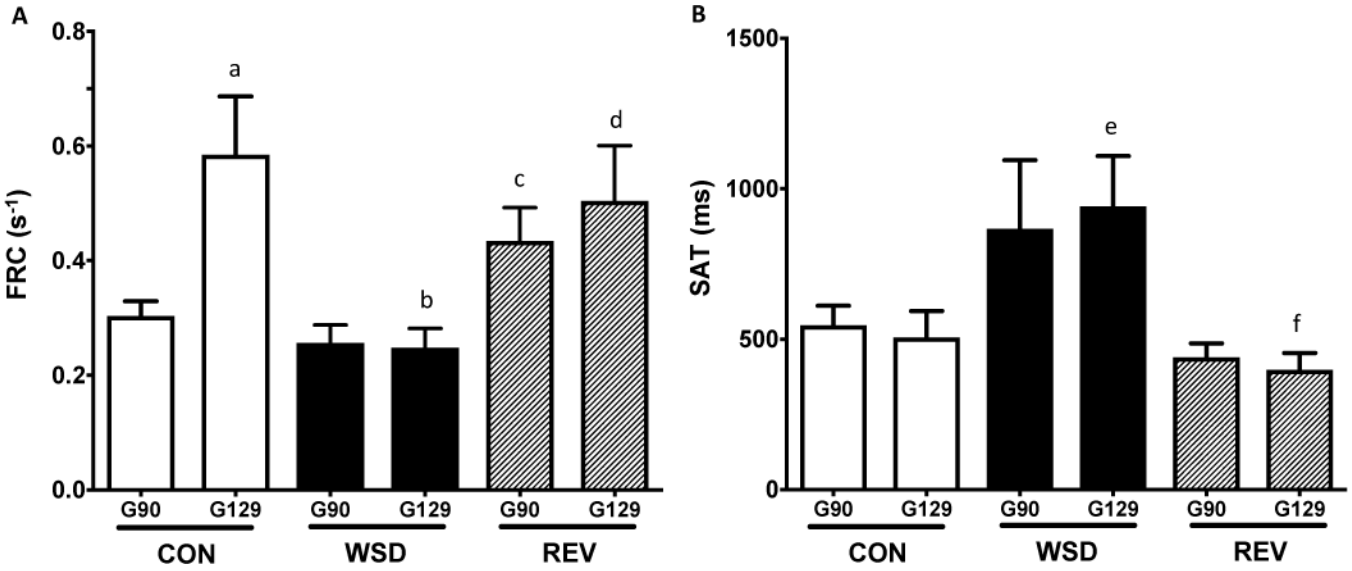

Figure 4. Contrast-Enhanced Ultrasound

A. Perfusion rate of the intervillous space (PRIVS, s^{-1}). B. Time to initial IVS perfusion (TIVSP, ms). [a]p<0.05 *vs.* G90, Mann-Whitney test; [b]p<0.001 *vs.* CON at G129; [c]p<0.05 *vs.* WSD at G90; [d]p<0.01 *vs.* WSD at G129; [e]p<0.01 *vs.* CON at G129; [f]p<0.001 *vs.* WSD at G129, Kruskal-Wallis test.

PRIVS, perfusion rate of the intervillous space; TIVSP, time from microbubble destruction to initial cotyledon filling.

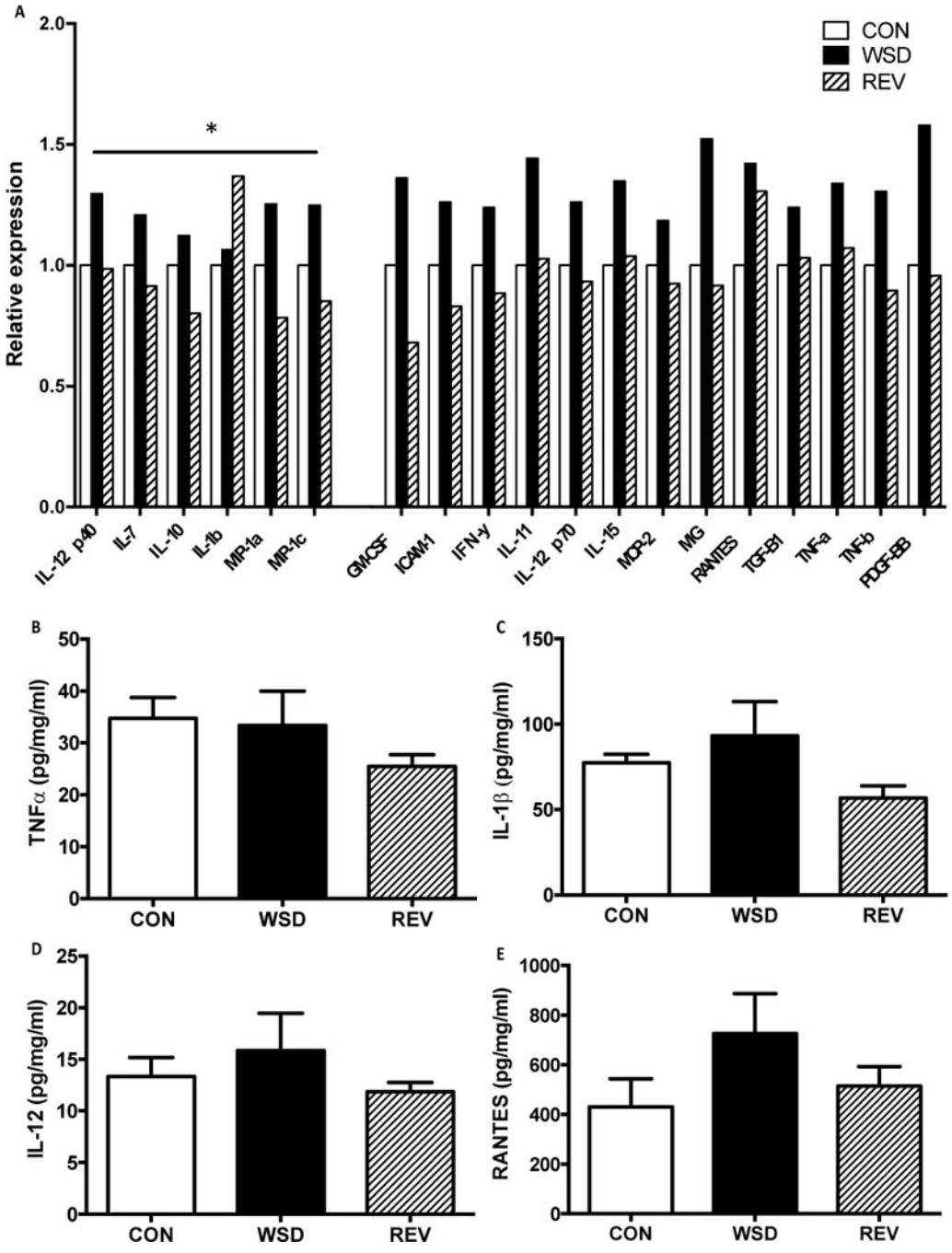

Figure 5. Placental inflammation

A. Protein expression levels of multiple inflammatory markers were assessed by antibody array. Protein expression was normalized to control levels. Inflammation was increased in the WSD cohort compared to controls, and decreased in the diet reversal cohort (*, <P=0.05, one-way ANOVA). B-E. Selected markers were investigated with ELISA, confirming lower levels of inflammatory markers in the diet reversal cohort compared to WSD. Comparisons amongst the 3 diet groups were made using a one-way ANOVA.

CON, control; WSD, Western-style diet; REV, diet reversal.

Table 1

Fetal and placental structural measurements.

Measurements	CON (n=6)	WSD (n=6)	REV (n=5)
Fetal weight (g)	340.8 ± 8.2	351.4 ± 8.0	367.2 ± 11.5
Placental weight (g)	106.3 ± 7.0	112.0 ±6.4	110.0 ± 5.3
Feto:placental weight ratio	3.1 ± 0.17	3.0 ± 0.17	3.4 ± 0.14
Placental volume (cm^3)	96.0 ± 4.1	99.2 ± 4.1	96.2 ± 4.7
Mean cotyledon number	11.3 ± 0.9	11.5 ± 0.9	12.3 ± 1.4
Mean cotyledon volume (cm^3)	9.5 ± 8.2	9.6 ± 8.2	8.5 ± 0.7
Intervillous space			
Volume fraction (%)	36 ± 0.7	37 ± 0.7	36 ± 0.7
Absolute volume (mm^3)	0.073 ± 0.003	0.075 ± 0.003	0.073 ± 0.004
Villous			
Volume fraction (%)	64 ± 0.7	63 ± 0.7	63 ± 0.8
Absolute volume (mm^3)	0.129 ± 0.0005	0.126 ± 0.0006	0.127 ± 0.0005
Fetal capillary absolute volume (mm^3)	0.093 ± 0.018	0.100 ± 0.019	0.108 ± 0.034
Trophoblast absolute volume (mm^3)	0.246 ± 0.038	0.207 ± 0.030	0.229 ± 0.009

Data are presented as mean ± standard error of the mean. CON, control; WSD, Western-style diet; REV, diet reversal.